Journal of Energy Chemistry 78 (2023) 1–12

Contents lists available at ScienceDirect

Journal of Energy Chemistry

journal homepage: www.elsevier.com/locate/jechem

http://www.journals.elsevier.com/journal-of-energy-chemistry/

Physics-informed neural network approach for heat generation rate estimation of lithium-ion battery under various driving conditions

Hui Pang, Longxing Wu *, Jiahao Liu, Xiaofei Liu, Kai Liu *

School of Mechanical and Precision Instrument Engineering, Xi'an University of Technology, Xi'an 710048, Shaanxi, China

ARTICLE INFO

Article history:
Received 11 October 2022
Revised 21 November 2022
Accepted 21 November 2022
Available online 28 November 2022

Keywords:
Lithium-ion batteries
Physics-informed neural network
Bidirectional long-term memory
Heat generation rate estimation
Electrochemical model

ABSTRACT

Accurate insight into the heat generation rate (HGR) of lithium-ion batteries (LIBs) is one of key issues for battery management systems to formulate thermal safety warning strategies in advance. For this reason, this paper proposes a novel physics-informed neural network (PINN) approach for HGR estimation of LIBs under various driving conditions. Specifically, a single particle model with thermodynamics (SPMT) is first constructed for extracting the critical physical knowledge related with battery HGR. Subsequently, the surface concentrations of positive and negative electrodes in battery SPMT model are integrated into the bidirectional long short-term memory (BiLSTM) networks as physical information. And combined with other feature variables, a novel PINN approach to achieve HGR estimation of LIBs with higher accuracy is constituted. Additionally, some critical hyperparameters of BiLSTM used in PINN approach are determined through Bayesian optimization algorithm (BOA) and the results of BOA-based BiLSTM are compared with other traditional BiLSTM/LSTM networks. Eventually, combined with the HGR data generated from the validated virtual battery, it is proved that the proposed approach can well predict the battery HGR under the dynamic stress test (DST) and worldwide light vehicles test procedure (WLTP), the mean absolute error under DST is 0.542 kW/m^3, and the root mean square error under WLTP is 1.428 kW/m^3 at 25 °C. Lastly, the investigation results of this paper also show a new perspective in the application of the PINN approach in battery HGR estimation.

1. Introduction

Energy crisis and environmental pollution provide a strong impetus for electrochemical energy storage systems used in various industries [1,2]. As a critical way to realize the electrification of transportation, vigorously developing electric vehicles (EVs) has become a universal consensus of various countries in the world. In this context, lithium-ion batteries (LIBs) are gradually becoming one of the most popular storage devices in the field of automotive applications [3]. However, the potential spontaneous combustion even thermal runaway risk of EVs has caused people to be anxious about the safety of LIBs [4]. To overcome this problem, accurate knowledge of battery thermal behaviors such as variation of temperature and heat generation rate (HGR) has become an important indicator to measure the effectiveness of battery thermal management (BTM) under different driving conditions [5].

Currently, many researchers have studied battery thermal behaviors by exploring the variation of surface and internal temperatures [6,7]. Although these results have provided important and strong support for improving the performance of BTM, it is reported that accurate insight into HGR may be another more essential factor than temperature for battery thermal failure [8]. Many studies also suggested that battery HGR is correlated with state of health parameters including cell impedance and electrode lithiation, which further emphasizes importance of battery HGR estimation [9]. In response to this, more and more attentions have been paid to quantitatively investigate and estimate battery HGR for improving the battery performance and associated fail-safe systems. According to the existing literature, there are three primary approaches to characterize battery HGR including experimental-based methods, model-based methods, and data-driven methods. Originally, some researchers mainly focused on the investigation of battery HGR by experimental measurements, such as accelerating rate calorimeter [10], isothermal heat conduction calorimetry [11]. Subsequently, although some different methods have been proposed to improve experimental efficiency and test accuracy of battery HGR [12], these experimental-based methods take enormous time cost and are only carried out in laboratory conditions, which makes it difficult to be applied in battery onboard usage scenarios.

* Corresponding authors.
E-mail addresses: batterywu@163.com (L. Wu), kliu@mail.xaut.edu.cn (K. Liu).

https://doi.org/10.1016/j.jechem.2022.11.036

Meanwhile, model-based methods can also be utilized for capturing the HGR variation of LIBs, and the current solutions mainly involve equivalent circuit model (ECM) [13] and electrochemical model (EM) [14]. Benefiting from simple structures, ECMs combined with Bernardi equations are broadly used to study the thermal behavior including battery HGR [15]. Nevertheless, since the ECMs do not consider physical properties of battery and Bernardi equations lack generalization capabilities [16,17], these methods are unable to account for the whole picture of battery HGR. In contrast, EMs can characterize the full electrochemical properties of the battery, which make it holding obvious advantages for capturing the HGR of LIBs. In this regard, Tahir et al. developed multiscale thermal model for high-power LIB to achieve the detailed HGR analysis [18]. Choe et al. studied the sensitivity of parameters to the battery HGR by the simplified EM and finished the parameters identification program [8]. These EM-based studies have provided in-depth insight into the variation of battery HGR, yet the tremendous computational burdens make battery EM prohibitive in actual on-board implementations. More importantly, the above-mentioned model-based methods just stayed at the level of open-loop computing, so they cannot realize the real-time feedback and correction of HGR for actual operation conditions of EVs. To this end, Wang et al. adopted an online HGR estimation based on simplified EM and dual-temperature measurements and the results indicated that this approach can estimate the HGR in real time [19]. Following closely behind, Jin et al. exploited the finite element method to address the inverse problem of energy conservation equation and proposed a novel algorithm for HGR and internal temperature estimation only by measuring the surface temperature of LIB [20]. Unfortunately, these two methods mainly focused on the investigation of HGR in battery constant charge/discharge cases, and the estimation availability of HGR under driving condition is not elaborated significantly. As the literature reported, the variations of HGR under complex driving conditions are more challenging to be evaluated accurately [21].

In contrast, the data-driven methods can well describe the nonlinear behavior between states variables of battery and sampled data, and it has the prominent advantage in adjusting their output results according to the onboard data collection, which circumvents cleverly the problems arising from the battery models [22]. At present, the data-driven methods have been widely applied in estimation of battery states [23], but only a few studies attempted to explore the potential of this method in battery HGR estimation. In this regard, Arora et al. made an artificial neural network (ANN) model to accomplish the HGR estimation of pouch cells under varied conditions [24]. Afterwards, in order to improve the estimation accuracy of single ANN method, Li et al. proposed a hybrid approach with ANN and extended Kalman filter to achieve the real-time prediction of battery HGR [25]. Nevertheless, these conditional ANN methods are limited in training time, and may involve a risk of overfitting. Particularly, the HGR of batteries has obvious time series characteristics while the traditional ANN has poor ability to handle these problems [26]. In this situation, the long short-term memory (LSTM) and derivative networks, which can avoid gradient explosion as the improved structure of recurrent neural network (RNN), and can much better solve these concerns [27,28]. Meanwhile, the pure data-driven models usually suffer from the unstable prediction results due to the lack of physics explanations. Facing this challenge, the physics-informed neural network (PINN) gradually attracted wide attention and stimulated the development of machine learning in battery states estimation fields [29,30]. One strategy for PINN method is to use physical models to provide additional, synthetic data to support data-driven model training [31]. For example, Li et al. established a PINN method to estimate the internal concentrations and potentials of both electrodes for LIBs and obtained desired results [32]. Yet, to the best of our knowledge, the investigations focusing on estimation of battery HGR with PINN approach are still in the research gap.

In order to address above concerns and further explore the application of PINN approach in battery HGR estimation, this paper innovatively applies this method to achieve the estimation of battery HGR under various driving conditions. Meanwhile, considering the time series characteristics of battery HGR, the Bayesian optimization algorithm (BOA)-based bidirectional LSTM (BiLSTM) network model is selected in PINN approach for improving the accuracy of HGR estimation. And the main contributions in this paper can be attributed to the following three aspects.

(1) The single particle model with thermodynamics (SPMT) is constructed to characterize the thermal behavior of LIBs while the critical physical knowledge related with HGR is analyzed.
(2) The solid surface concentrations obtained from SPMT are injected into the BiLSTM network model as physical information, which constitutes a novel PINN approach to achieve the HGR estimation of LIB, and its effectiveness is validated under typical driving conditions and ambient temperatures.
(3) The BOA is employed to figure out the hyperparameters selection problem of BiLSTM network used in PINN while the performance comparisons of three different LSTM networks for battery HGR estimation are conducted.

The remainder of this paper is organized as follows. Section 2 gives a detailed description of SPMT model in preparation for injecting the physical knowledge into BiLSTM network. A novel PINN framework for HGR estimation is proposed in Section 3. Section 4 displays the procedures of experimental tests and data collections. Then Section 5 provides the validated results and in-depth discussions. Finally, the conclusion of this paper is presented in Section 6.

2. The development of SPMT

It is well known that full-order pseudo two-dimensional (P2D) model with thermodynamics, as a typical representation of EMs, can well characterize the thermal characteristics of LIBs from the perspective of electrochemical mechanism, particularly the distribution of HGR [11]. However, the huge computational burdens prevent it from being used for estimation of actual battery HGR onboard. To provide physical knowledge related with battery HGR and leverage the EM for online application, here the SPMT model is utilized for characterizing the thermal behavior of batteries, which is shown in Fig. 1. It can not only explicitly provide the necessary physical knowledge and model fidelity, but also be capable of possessing the efficiency advantages of ECM [33]. The following section will further describe the construction process of SPM model and thermal model, respectively.

2.1. SPM model

According to the illustration on the left of Fig. 1, the SPM model abstracts the electrodes into two particles and assumes current density uniformly distributed. Therefore, the average bulk current density across the battery electrodes can be expressed by Ref. [34].

$$\bar{J}_p(t) = -\frac{I(t)}{AL_p} \tag{1}$$

$$\bar{J}_n(t) = +\frac{I(t)}{AL_n} \tag{2}$$

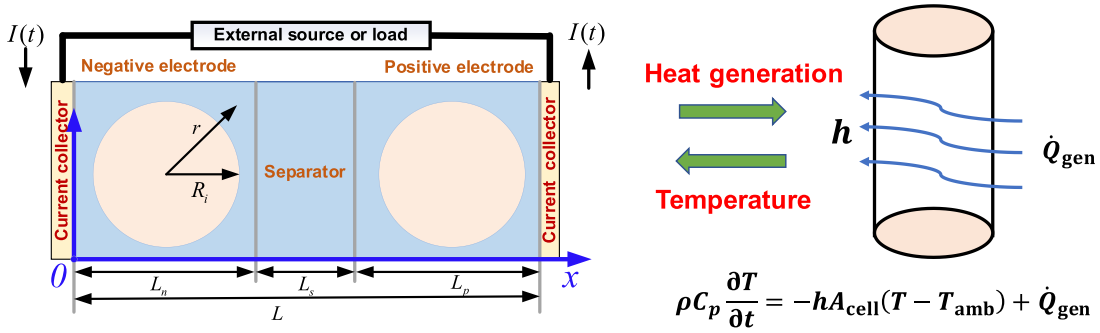

Fig. 1. The schematic diagram of SPMT model.

where $\bar{J}_i(t)(i=p,n)$ is the average current density across electrodes, p and n represent the positive and negative of electrodes, respectively. L_i denotes the thickness of electrodes. In addition, $I(t)$ is the applied current and A is the electrode plate area of battery.

Based on the above assumptions, the electrode solid-phase diffusion equations described in P2D model [35] can be expressed by

$$\frac{\partial c_{s,i}}{dt} = \frac{D_{s,i}}{r^2}\frac{\partial}{\partial r}\left(r^2\frac{\partial c_{s,i}}{\partial r}\right) \tag{3}$$

And the boundary conditions of Eq. (3) are listed below

$$\left.\frac{\partial c_{s,i}}{\partial r}\right|_{r=0} = 0, D_{s,i}\left.\frac{\partial c_{s,i}}{\partial r}\right|_{r=R_i} = \frac{\bar{J}_i(t)}{a_s F} \tag{4}$$

where $c_{s,i}$ presents the lithium-ion concentration of solid phase, $D_{s,i}$ is diffusion coefficient, R_i is solid-phase particle radius, a_s is specific surface area, and F is Faraday's constant.

On the other hand, the output voltage of the SPM model is expressed from the potential difference between the solid phase at the both end of electrodes [36].

$$V_{\text{cell}} = U_p(\theta_p) - U_n(\theta_n) + \eta_p - \eta_n - R_f\frac{\bar{J}_i(t)}{a_s} \tag{5}$$

Where V_{cell} is output voltage, R_f is film ohmic resistance, U_i is the open circuit potential of electrodes. And η_i is the overpotential of electrodes, θ_i represents the electrode utilization, which varies with the solid phase surface concentration $c_{s,i,\text{surf}}$. It should be noted that detailed information on obtaining $c_{s,i,\text{surf}}$ and V_{cell} can be found in Ref. [37].

2.2. Thermal model

Given that the SPMT model is mainly utilized for injecting essential physical information related with battery HGR into traditional data-driven networks, the lumped thermal model is considered as the best selection for achieving this function with lower computational burden. According to Ref. [38] and the illustration on the right of Fig. 1, the energy conservation equation can be written as

$$\rho C_p\frac{\partial T}{\partial t} = -hA_{\text{cell}}(T - T_{\text{amb}}) + \dot{Q}_{\text{gen}} \tag{6}$$

$$\dot{Q}_{\text{gen}} = I(t)(V_{\text{cell}} - U_p(\theta_p) + U_n(\theta_n)) + [-I(t)T(\frac{\partial U_p}{\partial T} - \frac{\partial U_n}{\partial T})] \tag{7}$$

where T_{amb} is the ambient temperature, A_{cell} is surface area of battery. ρ and C_p denote the density and the specific heat capacity of the battery, respectively. Besides, T is battery temperature, $\dot{Q}_{\text{gen}}$ is total heat generation, h is defined as convective heat transfer coefficient, $\partial U_i/\partial T$ and is the entropy variations of electrodes.

Ultimately, both the SPM and thermal models are coupled bidirectionally through HGR and temperature, and its schematic diagram is presented as shown in Fig. 1. Furthermore, all the parameters used in the SPMT model can be found in Section 4. As for the simulation effect and more governing equations of SPMT, many researchers have given the clear presentations in Ref. [33,39], which will not be repeated herein.

3. PINN framework for HGR estimation

3.1. BiLSTM network

It is well known that the HGR varies significantly with different the operating time of batteries, which has a distinct characteristics of time series. As a modified structure from RNN, the LSTM is one of most outstanding network architectures for dealing with nonlinear time series problems. With the help of one memory state and multiple gating functions, it is a fact that LSTM can effectively overcome gradient disappearance and explosion phenomenon in the process of network training so that it has advantages in remembering long range of information. Therefore, LSTM has been extensively studied in the field of states estimation of batteries [23,28]. Nevertheless, LSTM is also found to expose some limitations in recent years, which ignores the influence of future states on the current states and does not make full use of before-and-after dependencies of time series [40]. In this context, a new RNN structure, named BiLSTM network, emerges and enhances the prediction accuracy of traditional LSTM. Consequently, the BiLSTM network, as an alternative to the traditional LSTM, is used in our proposed PINN approach to achieve the estimation of battery HGR. As an illustration, the architecture relationships between BiLSTM and LSTM network are shown in Fig. 2. To better understand the working principle of BiLSTM, the LSTM needs to be described firstly.

As presented in Fig. 2, the forget gate f_t, input gate i_t and output gate o_t are contained in the basic unit of LSTM network, which makes LSTM possess the ability to recall the past information by executing an updating process from c_{t-1} to c_t. Particularly, the flow of information in LSTM network at time step t mainly consists of the following formulae as [40].

$$f_t = \sigma(W_f x_t + U_f h_{t-1} + b_f) \tag{8}$$

$$i_t = \sigma(W_i x_t + U_i h_{t-1} + b_i) \tag{9}$$

$$o_t = \sigma(W_o x_t + U_o h_{t-1} + b_o) \tag{10}$$

$$\tilde{c}_t = \tanh(W_c x_t + U_c h_{t-1} + b_c) \tag{11}$$

$$c_t = f_t \otimes c_{t-1} + i_t \otimes \tilde{c}_t \tag{12}$$

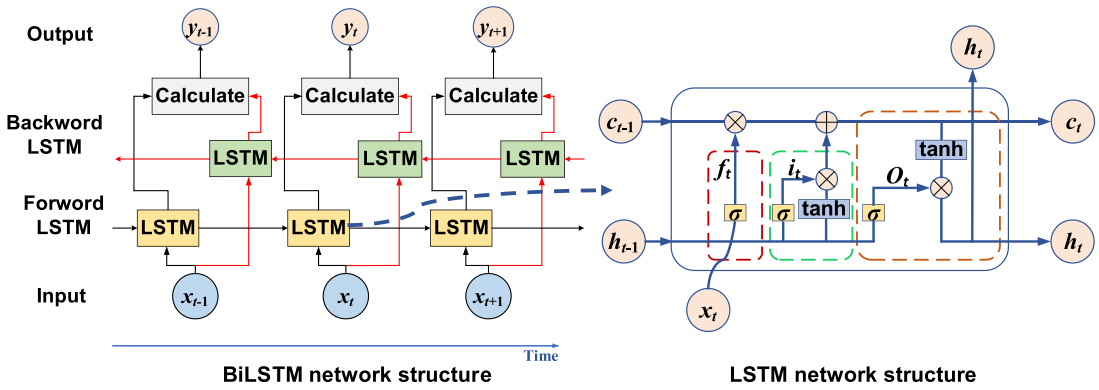

Fig. 2. Structure of LSTM and BiLSTM network.

$$h_t = o_t \otimes \tanh(c_t) \tag{13}$$

where x_t is the input variable of LSTM network at time t, h_t and h_{t-1} denote the output value of hidden layer at time t and time $t-1$, respectively. W_f, W_i, W_o, W_c, U_f, U_i, U_o, U_c are the weight matrixes obtained by networks training, b_f, b_i, b_o, b_c are bias vectors of every gate. σ and tanh represent the sigmoid function and tanh function, respectively. Besides, $\tilde{c}_t$ denotes the temporary input node and $\otimes$ is the element-wise multiplication.

Owing to using the forward and backward channels at one time, the BiLSTM network connects the hidden states of each position with two LSTM networks for calculating the final output y_t of network [41], as displayed in left of Fig. 2. For this reason, the BiLSTM network can take full advantages of the information contained in past and future moment data and receive the better prediction results. Combined with the unit information of LSTM, the forward hidden state $\overrightarrow{h}_t$ and backward hidden state $\overleftarrow{h}_t$ are expressed at time step t as follows.

$$\overrightarrow{h}_t = L\left(x_t, \overrightarrow{h}_{t-1}\right) \tag{14}$$

$$\overleftarrow{h}_t = L\left(x_t, \overleftarrow{h}_{t-1}\right) \tag{15}$$

$$y_t = W_{\overrightarrow{h}} \overrightarrow{h}_t + W_{\overleftarrow{h}} \overleftarrow{h}_t + b \tag{16}$$

where $W_{\overrightarrow{h}}$ and $W_{\overleftarrow{h}}$ are the weights matrixes of forward and backward LSTM networks, separately. b represents the bias vectors of output layer, and $L(\cdot)$ is the operation of LSTM network expressed in Eqs. (8)–(13).

3.2. BOA-based BiLSTM

It is reported that, different hyperparameter selections have a direct impact on the performance of network models, such as computational cost and prediction accuracy [42]. Generally, hyperparameters in RNN models are determined by trial-and-error methods, and their accuracy depends on the rules of thumb, which increases the burden of network training. Hence, BiLSTM network, like other architectures of RNN models, also needs to consider the hyperparameter optimization problems. Unlike grid search algorithm, the BOA keeps track of all the historical evaluations and it avoids the waste of computation to evaluate bad hyperparameters [43]. Simultaneously, the BOA does not have the parameter problem that exited in traditional population-based algorithms, such as particle swarm optimization, and is particularly useful when the calculation of the objective function is expensive [44]. As reported in the literature, the BOA can converge at optimized values in minimum number of iterations, which makes it widely used for addressing the issues of hyperparameters optimization [45]. Benefiting from this feature, the BOA is adopted here to compensate for the shortcoming of traditional trial-and-error methods in terms of the PINN-based battery HGR estimation.

Specifically, the core idea of BOA is to suppose probabilistic agent model of objective function $f(\boldsymbol{x})$, and this model is consistent with Gaussian process (GP) [45]. Consequently, BOA observes the prior probability of hyperparameters through the GP model to obtain a posterior probability distribution. After that, the GP model is constantly modified at each new the results of objective function $f(\boldsymbol{x})$ until the specified requirements are satisfied. Note that the relationship between the optimal hyperparameter set $\boldsymbol{x}^*$ and the objective function $f(\boldsymbol{x})$ is presented as follows.

$$\boldsymbol{x}^* = \operatorname{argmin}(f(\boldsymbol{x})); \boldsymbol{x} \in \boldsymbol{U} \tag{17}$$

where $\boldsymbol{x}$ is the set of parameters that need to be optimized, and $\boldsymbol{U}$ is the set of candidate parameters.

To sum up, the process of BOA-based BiLSTM hyperparameters selection can greatly reduce the training cost and guarantee that the final BiLSTM model has the better prediction accuracy. And further details on the optimization results of hyperparameters will be discussed in Section 5.

3.3. The PINN-based HGR estimation

This section proposes an innovative framework for real-time estimation of battery HGR based on PINN approach. Specifically, the first attempt is made to extract the physical variable associated with HGR in battery EM as the one input feature of BiLSTM network. It is helpful to enhance the generalization capability of battery HGR estimation because of the effective integration of physical knowledge and traditional BiLSTM network. To accomplish this goal, the deep insight into composition of the HGR from the perspective of electrochemical mechanism should be carried out. Obviously, the HGR of battery is mainly dependent on Eq. (7) and composed of reversible heat and irreversible heat. Although the lumped thermal model in Eq. (7) does not contain all the types of heat generation in battery EM, most studies have shown that it has occupied the main heat source of battery HGR [46,47], which is sufficient for extracting the main features that affect the variation of HGR. As can be seen from Eq. (7), in addition to the output voltage and applied current, the HGR value of the battery is also highly determined by $c_{s,i,\mathrm{surf}}$ in electrodes of solid phase, which inspires us to inject $c_{s,i,\mathrm{surf}}$ as the physical knowledge into BiLSTM networks for improving the accuracy of the PINN-based HGR estimation. In other words, there will be five feature variables $(I(t), V_{\mathrm{cell}}(t), T_{\mathrm{amb}}(t), c_{s,p,\mathrm{surf}}(t), c_{s,n,\mathrm{surf}}(t))$ as the input features for

the BiLSTM network used in PINN approach. Based on the above analysis, Fig. 3 shows the proposed framework of PINN-based HGR estimation of LIB.

It can be observed from Fig. 3, the framework of PINN-based HGR estimation of battery mainly consists of data acquisition, PINN framework, and results prediction. In addition to data acquisition and outcome prediction, the construction of proposed PINN needs to be given more information during the battery HGR estimation. And the proposed PINN framework mainly consists of SPMT model and BOA-based BiLSTM network. To be specific, the function of SPMT model is to provide the real-time variables including $c_{s,p,\mathrm{surf}}$ and $c_{s,n,\mathrm{surf}}$ related with HGR, which makes BiLSTM infused with physics-informed features and is also a key difference from other traditional BiLSTM models. As for the BiLSTM network, the input layer, hidden layer (BiLSTM), full connection layer and output layer form the network structure of battery HGR estimation. In fact, the BiLSTM network serves as the main subject of PINN to train the network data and estimate HGR of battery. Hence, the dataset utilized for training the BiLSTM network is presented by

$$D = \{(\boldsymbol{x}_1, \boldsymbol{y}_1), (\boldsymbol{x}_2, \boldsymbol{y}_2), \cdots, (\boldsymbol{x}_k, \boldsymbol{y}_k)\} \tag{18}$$

where $\boldsymbol{y}_k$ here denotes the values of HGR at time step k. Besides, $\boldsymbol{x}_k$ presents the input vector at time step k and here $\boldsymbol{x}_k = [I(t),\ V(t),\ T_{\mathrm{amb}}(t),\ c_{s,p,\mathrm{surf}}(t), c_{s,n,\mathrm{surf}}(t)]$.

Additionally, to further illustrate the role of BOA in BiLSTM network, three hyperparameters including number of hidden units, initial learning rate and L2-regularization are chosen as objects for optimization, which is mainly based on the following considerations.

Hidden units: This hyperparameter corresponds to the amount of information remembered between time-steps. If the number of the hidden unit is too small, the information acquisition required by the sample training process cannot be satisfied. On the contrary, the overfitting will occur, resulting in a decrease in the generalization ability of the network [48].

Initial learning rate: This hyperparameter is used for training the algorithm. Too low learning rate takes a long training time and too high learning rate might conclude at a suboptimal result or diverge [49].

L2-regularization: It corresponds to the weight decay factor that is responsible to reduce training data overfitting [50].

Meanwhile, search bounds of those three hyperparameters are determined in conjunction with the relevant literatures [48,51] and are listed in Table 1. It is noted that, the number of iterations here is set as the cut-off condition for the process of BOA.

In conclusion, the proposed method particularly allows the BiLSTM network to associate the EM's inherent physical states $(c_{s,p,\mathrm{surf}}(t), c_{s,n,\mathrm{surf}}(t))$ with measurement data for building a novel PINN framework, thus greatly enhancing the predictive accuracy of battery HGR. Then, the detailed execution steps of proposed PINN approach are as follows.

Step 1. Data pre-processing: To train and test the BiLSTM network used in the PINN method for battery HGR estimation, five dynamic driving conditions are carried out to collect the data of HGR in turn under the temperature of 25 °C and 35 °C. Considering the normalizing the collected data is a prerequisite for building and training BiLSTM network, here the function of mapminmax, as expressed in Eq. (19), is used to map collected data to the interval of [0,1]. Meanwhile, these normalized data are divided into training the data and test data. More detailed source and processing of data can be found in subsection 4.2.

$$z^* = \frac{z - z_{\min}}{z_{\max} - z_{\min}} \tag{19}$$

where z^* is normalized battery data, z is the raw data collected. $z_{\max}$ and $z_{\min}$ are the maximum and minimum values of the collected data, respectively.

Step 2. Hyperparameters optimization: The BOA is utilized for selecting the appropriate hyperparameters including number of hidden units, initial learning rate and L_2-regularization, which is described in subsection 3.2.

Step 3. Construction and training of BiLSTM: The composition sequence of four layers, determined hyperparameters and Adam optimization algorithm are used to construct and train the BiLSTM network.

Step 4. Performance evaluation: For the purpose of evaluating the performance of the PINN described above, two error indicators including the root means square error (RMSE) and the mean absolute error (MAE) are chosen. The reason for using them is that MAE

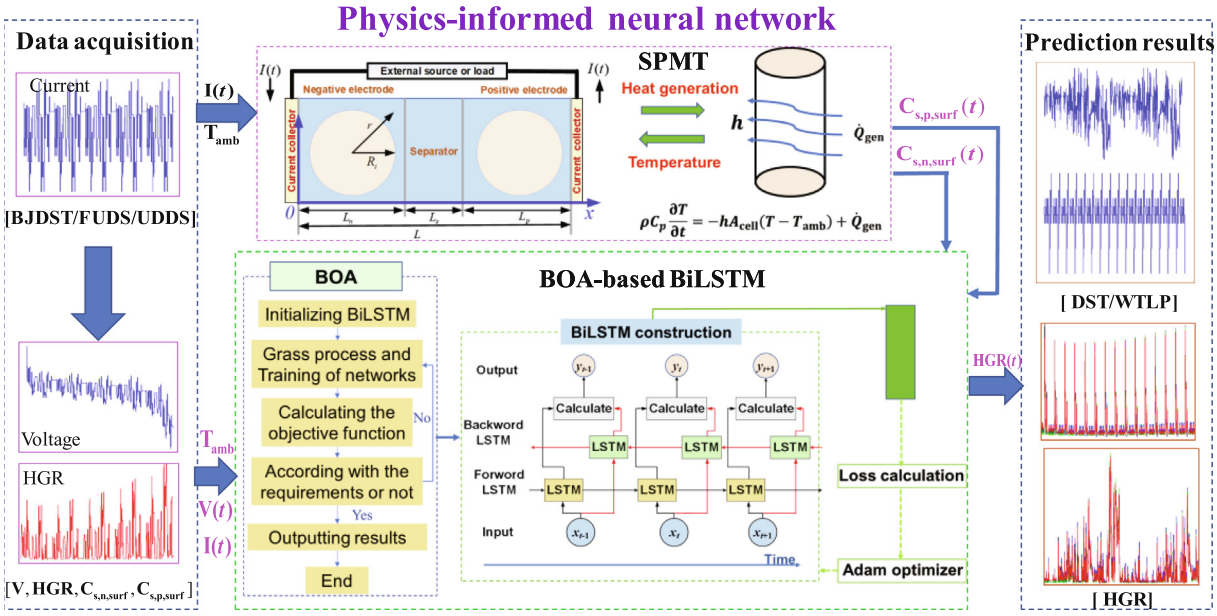

Fig. 3. The framework of PINN-based HGR estimation of battery.

Table 1
Optimized hyperparameters and the corresponding search bounds.

Hyperparameters	Search bounds
Number of hidden units	[90,150]
Initial learning rate	[1e − 8,1e − 1]
L2-regularization	[1e − 8,1e − 3]

can better reflect the reality of the estimation error, while RMSE can better give the impact of abnormal results [52]. Then these two evaluation criteria are explained below.

$$\mathrm{RMSE} = \sqrt{\frac{1}{n}\sum_{k=1}^{n}(\hat{y}_k - y_k)^2} \tag{20}$$

$$\mathrm{MAE} = \frac{1}{n}\sum_{k=1}^{n}|\hat{y}_k - y_k| \tag{21}$$

where $\hat{y}_k$ and y_k are the estimated HGR and real HGR at k th sample time, respectively. n denotes the total time number of samples.

4. Experiment and data description

In this section, a cylindrical LiFePO4 battery cell with nominal capacity of 2.3 Ah is used to validate the thermal behavior of virtual battery created by COMSOL Multiphysics 5.6. Studies have indicated that these Multiphysics coupling models for battery are increasingly dominant in characterizing the variation of hard-to-measure HGR [53]. Therefore, the validation of the virtual battery is important to generate the usable HGR data. However, it should be noted that there are still some differences between virtual battery and experimental batteries, hence the errors of battery HGR estimation resulting from this difference was not within the scope of discussion in this paper. In addition, the parameters required by virtual battery can be found in Refs. [54,55].

4.1. Experimental test

This paper mainly focuses on the HGR state of batteries in actual operating conditions, where the discharge current occupies the main part. Meanwhile, some facts have also been reported that: (1) The allowable maximum charging current is ordinarily lower than the discharging current; (2) Battery HGR is considerably decreased under charging at the same current conditions [56]; (3) Discharge is uncertain and determined by the power demands of EV, whereas charge is in a fixed mode [57]. Consequently, the thermal characteristic experiments of battery during the discharge condition are carried out in this paper.

To collect the experiment data of voltages and cell temperatures under the different conditions, a battery experimental bench is set up, as displayed in Fig. 4(a). Specifically, it mainly consists of a battery test system (ITECH-ITS5300), a thermal-controlled chamber (HYD-TH-80DH), two type-T thermocouples (GG-K-30), some test wires and a host personal computer. Based on this, a series of battery thermal characteristics experiments under various currents (1 C/2 C/3 C) and ambient conditions (25 and 35 °C) are carried out. To facilitate illustration, Fig. 4(b) takes the temperature of 25 °C as an example to show the test procedure of battery under various discharge C-rates. Similarly, the characteristic curves of battery at the operation temperature of 35 °C can be acquired by repeating the steps in Fig. 4(b). More experimental details for data access can be found in Ref. [58].

Subsequently, these collected experimental data are utilized for verifying the voltages and temperatures response of the virtual battery. It can be clearly observed from Fig. 5(a and c) that the voltage variations from the adopted virtual battery are consistent with the experimental data generated from multiple discharge C-rates. As for the variation of temperature, although there are fluctuations in simulant temperature curves in Fig. 5(b and d), the virtual battery has captured the major trend in temperature response as well as these fluctuations are kept within the acceptable limits. Thus, the virtual battery can be employed for collecting the data of HGR under different driving conditions and evaluating the results of HGR estimation in subsequent research.

4.2. Data acquisition of battery HGR

To evaluate the effectiveness of the proposed PINN method for battery HGR estimation, it is imperative to collect the battery datasets under several driving conditions. Particularly, it is very difficult to measure HGR(t) in practice, so it needs to be obtained by the experimentally validated virtual battery. Additionally, inspired by Ref. [59], here the training data of $c_{s,p,\mathrm{surf}}(t)$ and $c_{s,n,\mathrm{surf}}(t)$ generated by virtual battery are not used as the training set. Instead, the dataset of $c_{s,p,\mathrm{surf}}(t)$ and $c_{s,n,\mathrm{surf}}(t)$ obtained from the SPMT model under the same input conditions as the virtual battery are applied as the input of BiLSTM network for training, which is helpful to avoid HGR fluctuations caused by deviations in solid phase concentrations.

Considering these factors, five dynamic driving conditions including Beijing dynamic stress test (BJDST), federal urban driving schedule (FUDS), urban dynamometer driving schedule (UDDS), dynamic stress test (DST), worldwide light vehicles test procedure (WLTP) are carried out to collect the data of battery HGR in turn under the temperature of 25 and 35 °C. Different from those that training and testing networks at different proportions using the same dataset, this paper considers the 80% data from the BJDST, FUDS and UDDS as training set of BiLSTM network and 20% data from that as validation dataset of BiLSTM network. Such design scheme for training set helps to enhance the generalization ability of the proposed PINN in estimating battery HGR [60]. Although these conditions (BJDST, FUDS and UDDS) are selected for training dataset randomly, it still needs to be emphasized that, this selection should preferably include more variation ranges of dynamic current. At the same time, all the data collected under the DST and WLTP conditions will be applied as the testing dataset to estimate battery HGR results. To further have an insight into the HGR characteristics of LIB under the these driving conditions, Fig. 6 shows the input currents and HGR variations of the BJDST, FUDS and UDDS under the temperature of 25 °C. It is worth mentioning that, the input currents used for these driving conditions are obtained by scaling with proportions according to the methods described in Ref. [61].

5. Results and discussion

In this section, the prediction results of battery HGR using the PINN under different driving conditions are evaluated, while the accuracies of LSTM, BiLSTM and BOA-based BiLSTM used in PINN approach are compared at 25 °C. Meanwhile, the optimized hyperparameters of the BiLSTM network by BOA and the other parameters used in three selected networks are listed in Table 2. Besides, the training and testing of networks under the same conditions are carried out. Note that the construction and analysis of these networks are completed using MATLAB R2021b software.

5.1. Battery HGR estimation with PINN

Considering the adaptability of PINN-based battery HGR estimation, two driving conditions (DST and WLTP) are selected to verify the accuracy of this method. And the estimated results of

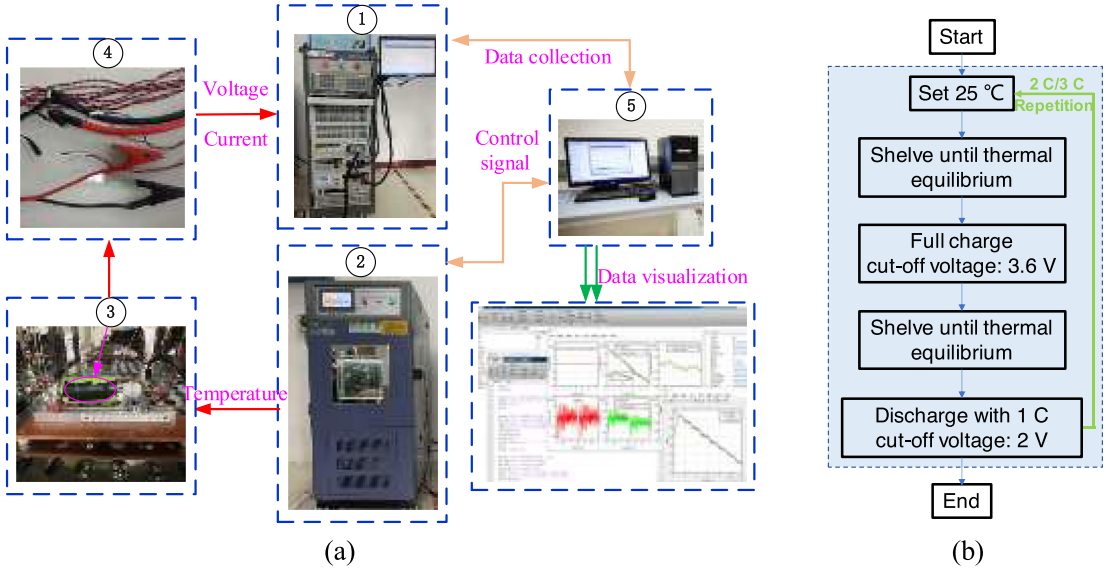

Fig. 4. Experimental bench and procedure for testing battery. (a) Experimental bench; (b) experimental procedure.

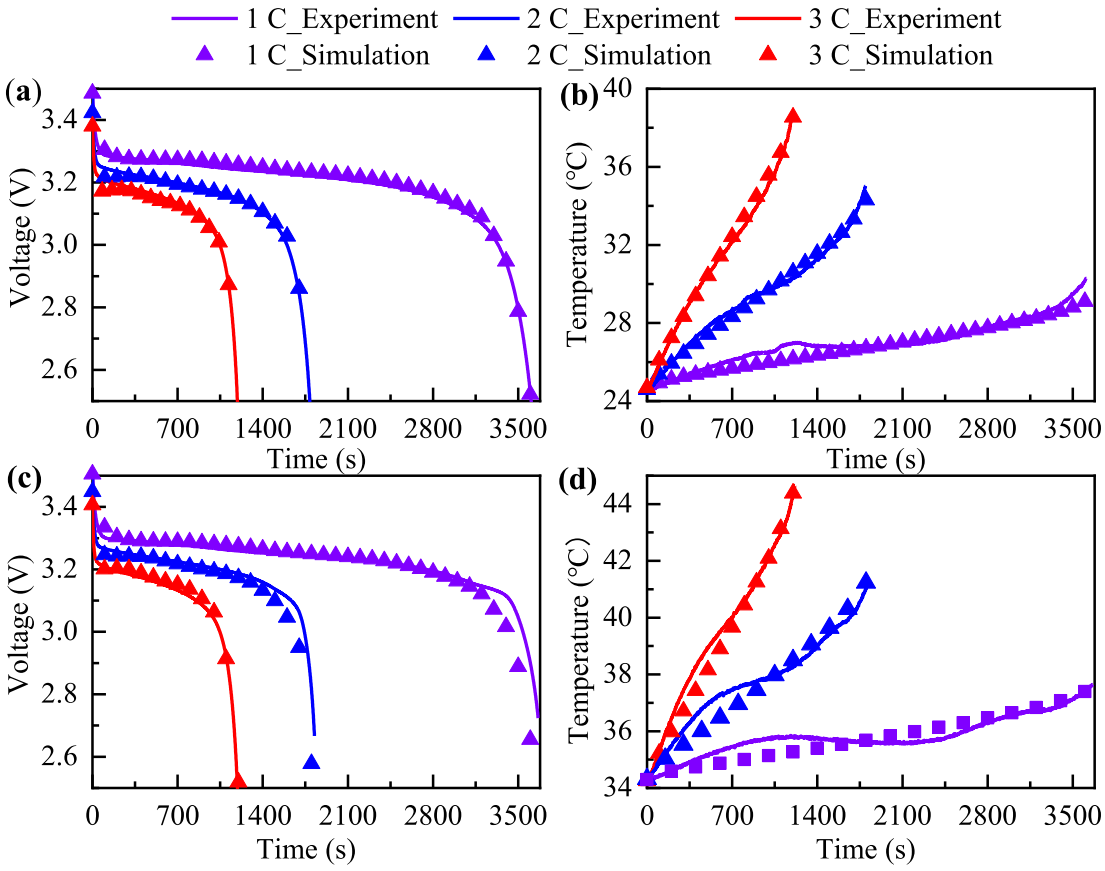

Fig. 5. The comparison between experimental results and simulative results. (a) Voltage responses under 25 °C; (b) temperature profiles under 25 °C; (c) voltage responses under 35 °C; (d) temperature profiles under 35 °C.

battery HGR using PINN under the temperature of 25 °C are depicted in Fig. 7.

It can be observed from Fig. 7(a and b), under DST and WLTP conditions, the estimated HGR using proposed PINN can well track the variations of actual HGR generated from virtual battery. In order to obtain more clear view, partial estimation results of two driving cycles are selected and given in Fig. 7(c and d). Obviously, the estimated HGR almost coincides with actual HGR except for some scattered points of current mutation. This conclusion can also be supported in the error curves shown in Fig. 7(e and f). Specifically, the absolute error (AE) for estimated HGR under DST condition is generally kept within ± 3 kW/m^3 apart from a few points,

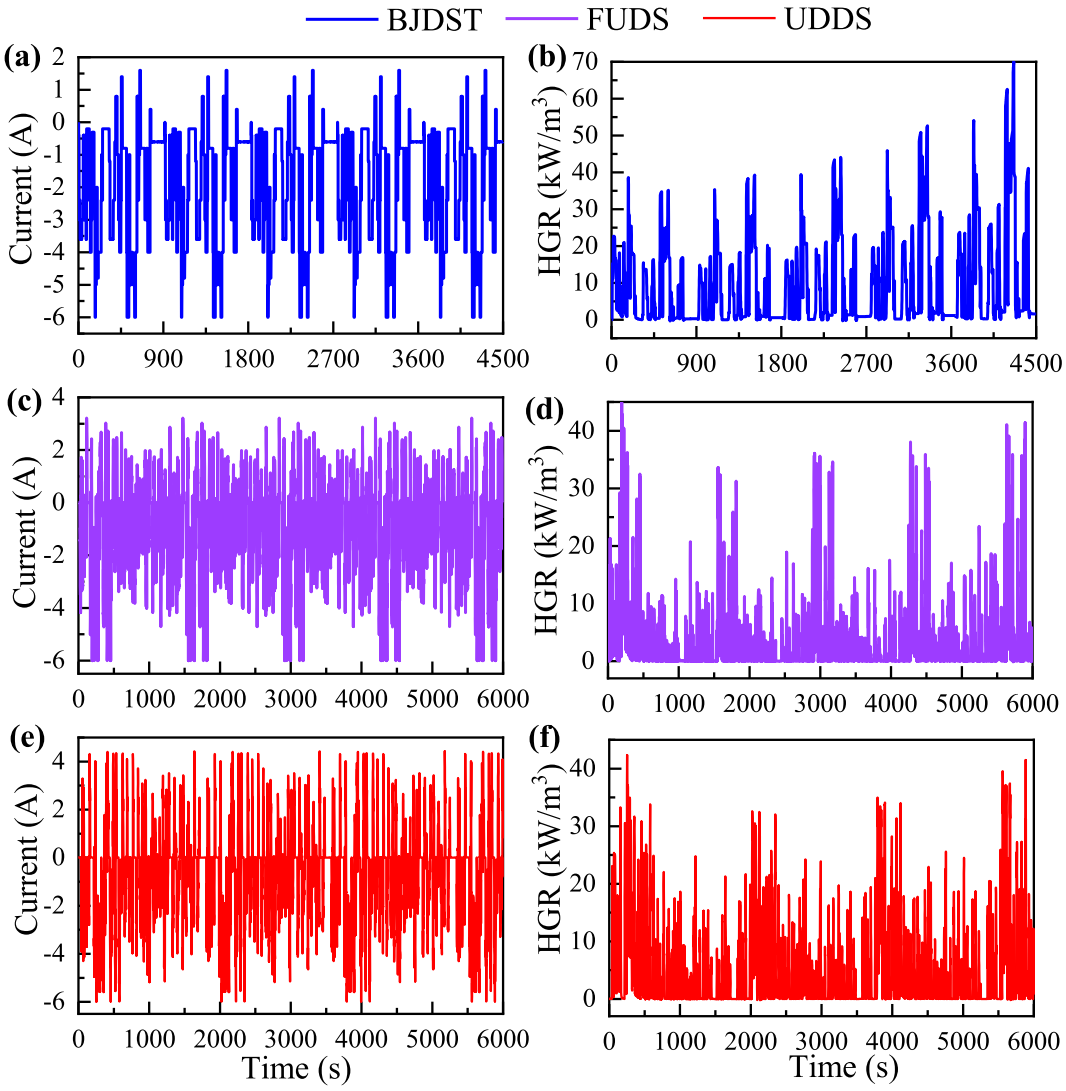

Fig. 6. Curves of the currents and HGRs under different driving conditions. (a, b) BJDST; (c, d) FUDS; (e, f) UDDS.

Table 2
Main hyperparameters and optimization algorithm in selected network models.

Hyperparameters	Network models used in PINN approach for HGR estimation			
	LSTM (25 °C)	BiLSTM (25 °C)	BOA-based BiLSTM (25 °C)	BOA-based BiLSTM (35 °C)
Number of hidden units	80	80	129	144
Initial learning rate	1e − 2	1e − 2	2.81e − 6	2.93e − 7
L2-regularization	1e − 4	1e − 4	3.03e − 8	5.18e − 3
Number of iterations	150	150	150	150
Optimization algorithm	Adam	Adam	Adam	Adam

while the AE under WLTP condition is relatively high but is still maintained in ± 4 kW/m^3.

Similarly, Fig. 8 gives the estimation results of battery HGR at 35 °C for further illustrating the applicability of the PINN approach when subjected to temperature variations. It can be concluded from Fig. 8(a and b) that the AE fluctuations of the HGRs at 35 °C increase compared with that at 25 °C, but this does not affect its overall capture of the battery HGR trend. That is to say, the AE of estimated HGR under DST varies generally from − 3 and 4 kW/m^3, and the AE at WLTP is between − 2 and 5 kW/m^3. Fortunately, these AEs are still within acceptable ranges with respect to the values of total battery HGR. And the above descriptions about the AE of battery HGR can be found in Fig. 8(e and f).

To further analyze the accuracy of the PINN approach for battery HGR estimation, Fig. 9 shows the MAEs and RMSEs of the estimated HGRs under DST and WLTP conditions. As for the evaluations at 25 °C, the MAE of estimated HGR under DST is smaller than that obtained from WLTP, and they are 0.542 and 0.924 kW/m^3, respectively. In contrast, the MAE and RMSE of HGR estimation are increased at 35 °C. Taking the RMSE of estimated HGR as an example, they are given as 1.053 and 1.499 kW/m^3, which reveals that the PINN-based method can

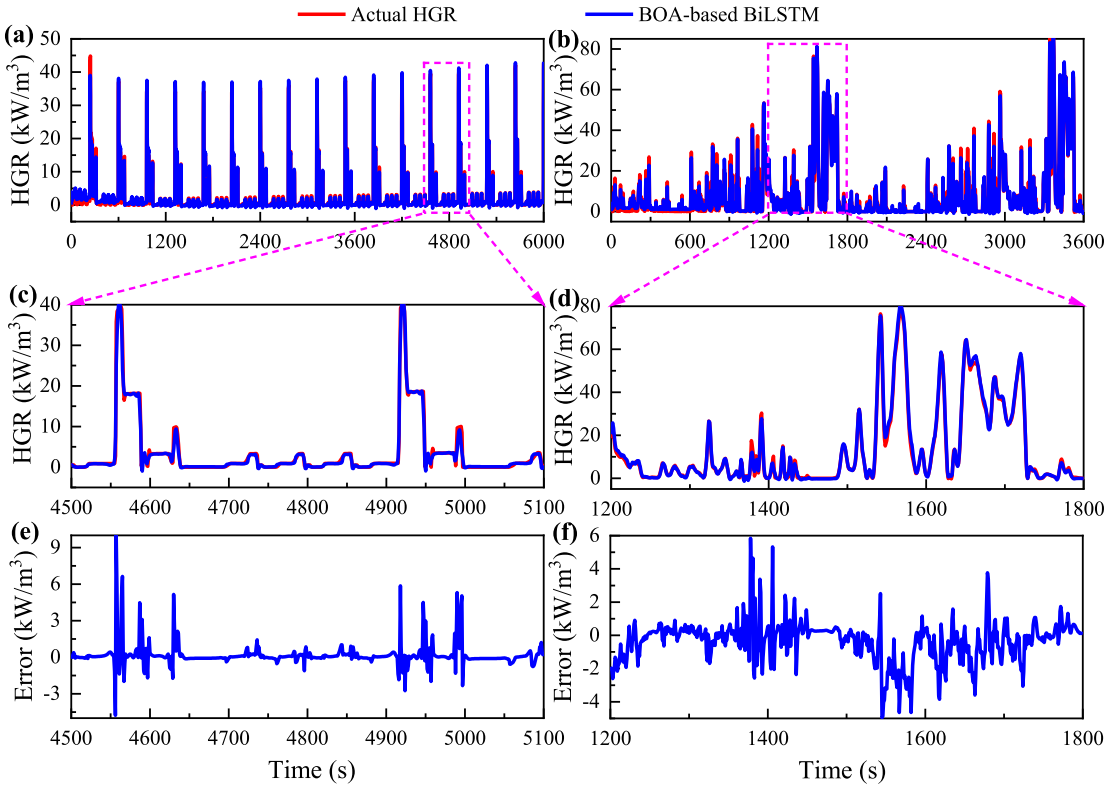

Fig. 7. Results of battery HGR estimation using PINN at 25 °C. (a) DST; (b) WLTP; (c, e) Partial profiles of DST; (d, f) partial profiles of WLTP.

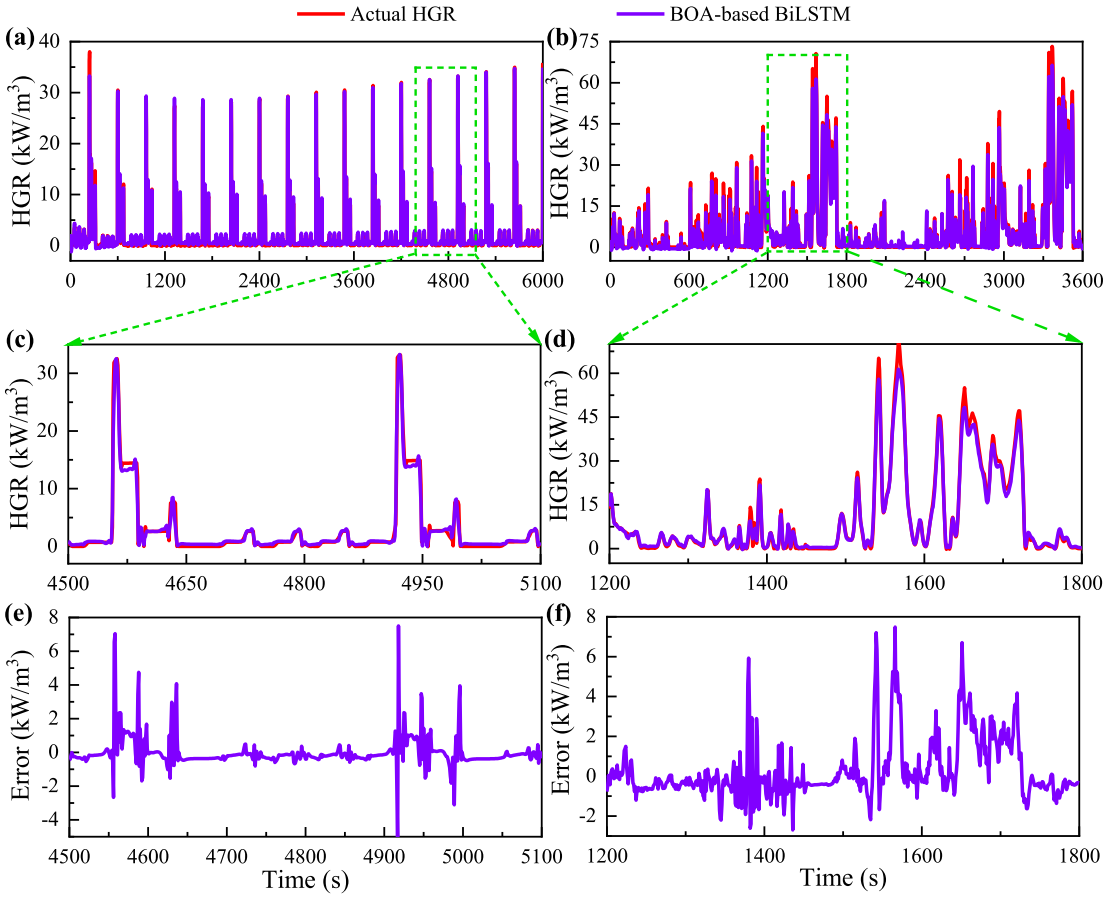

Fig. 8. Results of battery HGR estimation using PINN at 35 °C. (a) DST; (b) WLTP; (c, e) partial profiles of DST; (d, f) partial profiles of WLTP.

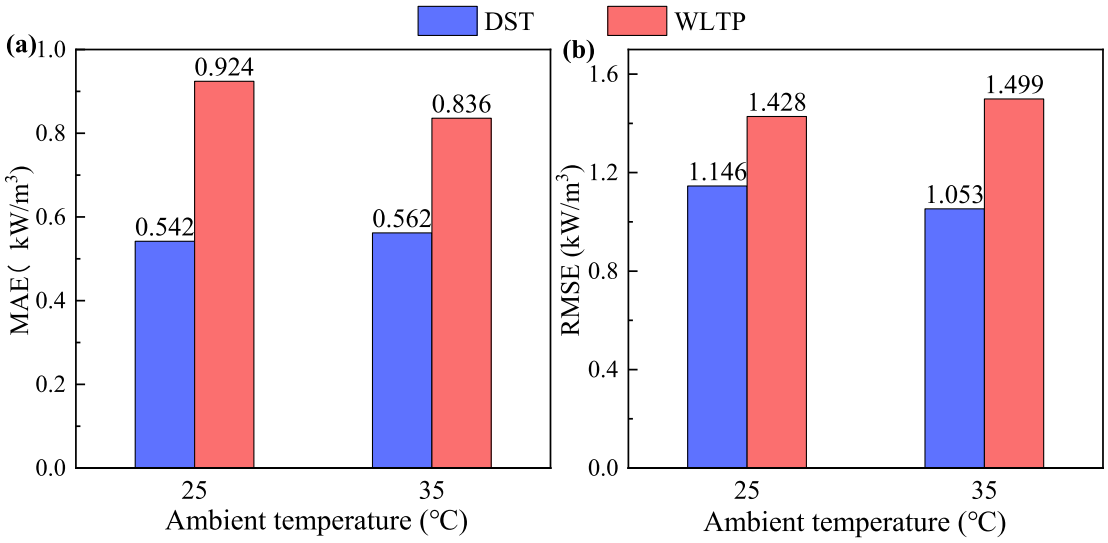

Fig. 9. Results of battery HGR estimation using PINN approach under the conditions of DST and WLTP. (a) MAE; (b) RMSE.

achieve good results overall in the HGR estimation although there are some error fluctuations.

5.2. Comparisons of other LSTM networks

To better demonstrate the superiority of the BOA-based BiLSTM network used in PINN framework, the performance comparisons in battery HGR estimation using three different network models, namely LSTM, BiLSTM and BOA-based BiLSTM at 25 °C are presented herein. Fig. 10 displays the battery HGR results estimated by LSTM, BiLSTM and BOA-based BiLSTM under DST and WLTP conditions.

Although all three network models can track the trend of HGR changes, as shown in Fig. 10(a and b), the BOA-based BiLSTM gives closer results to the actual HGR than LSTM and BiLSTM network. For example, as can be seen in Fig. 10(c and d), the HGR results

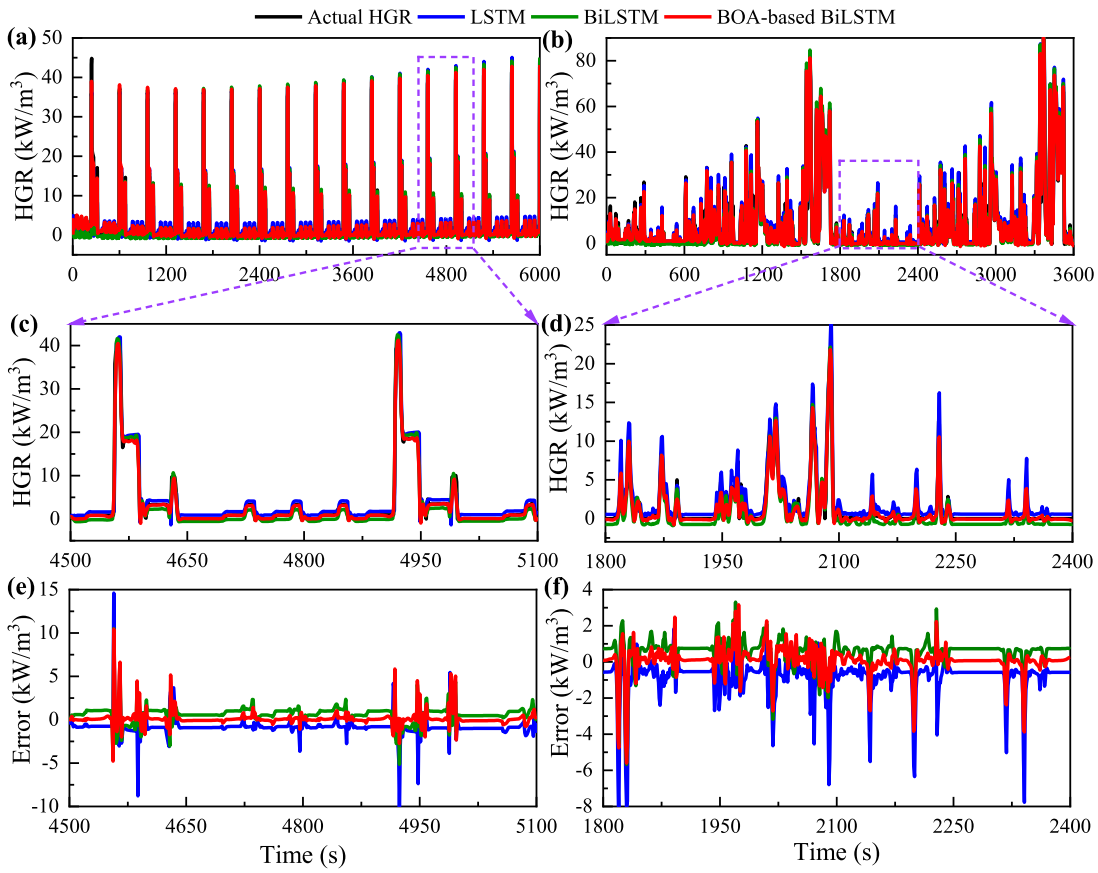

Fig. 10. Comparison of HGR estimation results using three network models at 25 °C. (a) DST; (b) WLTP; (c, e) partial profile of DST; (d, f) partial profile of WLTP.

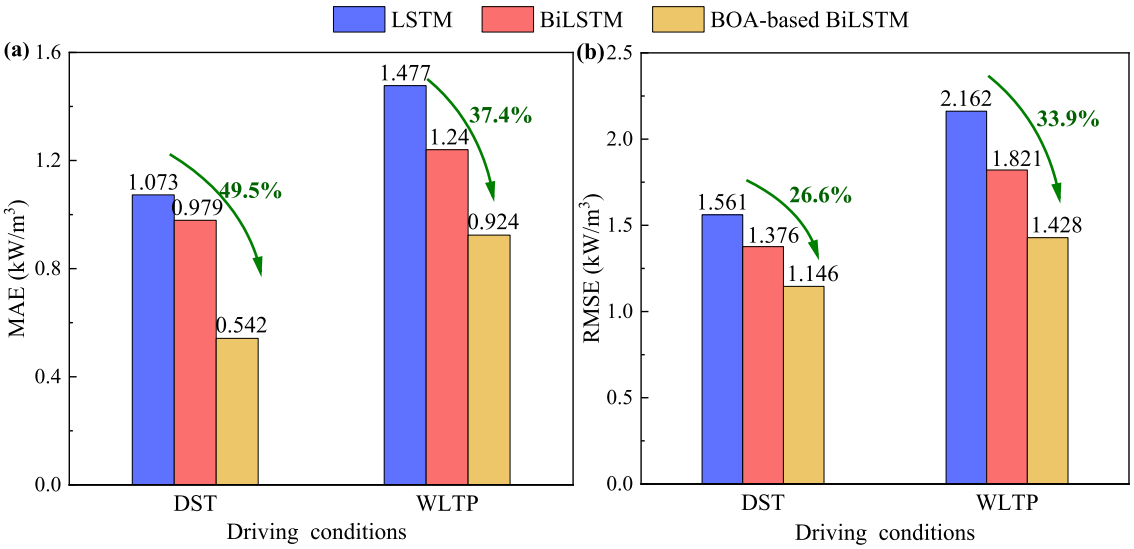

Fig. 11. Comparison of battery HGR estimation using three network models in PINN at 25 °C. (a) MAE; (b) RMSE.

estimated by BOA-based BiLSTM can keep up with the actual HGR with faster speed both under DST and WLTP conditions, which are benefited from the abilities to bidirectionally learning the feature series and optimizing hyperparameters of BiLSTM for battery HGR. As observed in Fig. 10(e and f), the LSTM-based HGR estimation has the higher error fluctuations and larger local AEs in the event of sudden current changes. On the contrary, the BOA-based BiLSTM battery HGR estimation can make the error range kept with ± 2 kW/m^3 on the whole. In case of BiLSTM, the estimation results are much better than the LSTM but not good as the BOA-based BiLSTM, which is attributed to the setting of hyperparameters.

To facilitate comparison and observations, more detailed MAEs and RMSEs of three network models used in PINN have been described in Fig. 11. Specifically, the MAE and RMSE from the LSTM under DST condition are 1.073 and 1.561 kW/m^3 and these indices are calculated as 1.477 and 2.162 kW/m^3 under WLTP conditions. Compared with the LSTM, the MAE and RMSE from the BOA-based BiLSTM have much better results. For example, they are decreased by 49.5% and 26.6% under the DST condition, separately. As a result, these investigations further indicate that the BOA-based BiLSTM can obtain better accuracy in PINN framework for battery HGR estimation under various driving conditions.

During the application of the PINN approach for battery HGR estimation under the actual battery operation, the trained BOA-based BiLSTM can map battery's real-time acquisition of variables $(I(t), V_{\text{cell}}(t), T_{\text{amb}}(t), c_{s,p,\text{surf}}(t), c_{s,n,\text{surf}}(t))$ at time step k directly to its HGR the current time step k, thus realizing the expected HGR estimation on board. Therefore, the proposed PINN approach in this paper can be achieved for estimating the battery HGR under the various driving conditions.

6. Conclusions

In this paper, a novel PINN approach for HGR estimation of LIBs under various driving condition is proposed. First, SPMT model that is suitable for injecting the physical features related to HGR is established. Then, combined with the physical features and BiLSTM network, a PINN framework for HGR estimation is constructed. Afterwards, the BOA is applied to determine critical hyperparameters for BiLSTM. Based on this, the proposed PINN can well realize the battery HGR estimation under DST and WLTP conditions. Additionally, the accuracy comparisons of LSTM, BiLSTM and BOA-based BiLSTM in estimating the battery HGR are also performed. Finally, the results have revealed that the proposed PINN approach has good performance on battery HGR estimation, and the MAE under DST is 0.542 kW/m^3 and RMSE under WLTP is 1.428 kW/m^3. Based on these, the major innovations of proposed PINN method for battery HGR estimation in this paper compared with previous literatures are mainly reflected in the three aspects: (1) PINN method can extract features related with HGR from measured data and physics-based model simultaneously, which satisfy the constraints of physical interpretability compared with traditional data-driven approach; (2) PINN method applies the BOA-based BiLSTM network model to estimate the battery HGR, which can improve the HGR estimation accuracy; (3) PINN method can well realize battery HGR estimation under various driving conditions.

Additionally, future work will focus on the more collection of real experimental data to verify the reliability of the virtual battery and the PINN-based HGR estimation. And the battery HGR characteristics under charging conditions have been also considered in our next step of research.

Declaration of competing interest

The authors declare that they have no known competing financial interests or personal relationships that could have appeared to influence the work reported in this paper.

Acknowledgments

This research was funded by the Artificial Intelligence Technology Project of Xi'an Science and Technology Bureau in China (No. 21RGZN0014).

References

[1] Z. Zhang, Q. Wang, Z. Liu, Q. Chen, Z. Guo, H. Zhang, Appl. Energy 329 (2023).
[2] Z. Huang, A. Mu, L. Wu, B. Yang, Y. Qian, J. Wang, ACS Sustain. Chem. Eng. 10 (2022) 7786–7810.
[3] R. Wang, C. Song, W. Huang, J. Zhao, Int. J. Electr. Power Energy Syst. 137 (2022).
[4] T. Shan, Z. Wang, X. Zhu, H. Wang, Y. Zhou, Y. Wang, J. Zhang, Z. Sun, J. Energy Chem. 72 (2022) 241–257.
[5] W. Zhang, W. Wan, W. Wu, Z. Zhang, X. Qi, Appl. Therm. Eng. 212 (2022).

[6] H. Pang, L. Guo, L. Wu, J. Jin, F. Zhang, K. Liu, J. Energy Storage 41 (2021).
[7] H. Shi, S. Wang, C. Fernandez, C. Yu, W. Xu, B. Dable, L. Wang, Appl. Energy 324 (2022).
[8] M. Song, S.Y. Choe, Appl. Energy 305 (2022).
[9] J. Marcicki, X. Yang, J. Electrochem. Soc. 161 (2014) A1794-A1800.
[10] Y. Hu, S.Y. Choe, T.R. Garrick, J. Power Sources 532 (2022).
[11] E. Schuster, C. Ziebert, A. Melcher, M. Rohde, H. Seifert, J. Power Sources 286 (2015) 580–589.
[12] L. Giammichele, V.D. Alessandro, M. Falone, R. Ricci, Appl. Therm. Eng. 205 (2022).
[13] X. Hu, S. Li, H. Peng, J. Power Sources 198 (2012) 359–367.
[14] C. Li, N. Cui, C. Wang, C. Zhang, Energy 221 (2021).
[15] Y. Bai, L. Li, Y. Li, G. Chen, H. Zhao, Z. Wang, C. Wu, H. Ma, X. Wang, J. Energy Chem. 29 (2019) 95–102.
[16] P. Jindal, R. Katiyar, J. Bhattacharya, Appl. Therm. Eng. 201 (2022).
[17] X. Hu, X. Deng, F. Wang, Z. Deng, X. Lin, R. Teodorescu, Proc. IEEE 110 (2022) 735–753.
[18] M.W. Tahir, C. Merten, Energy Convers. Manag. 258 (2022).
[19] J. Zhang, X. Yang, F. Sun, Z. Wang, C. Wang, Appl. Energy 272 (2020).
[20] P. Qin, S. Wang, Y. Cheng, L. Jiang, Q. Duan, K. Jin, Q. Wang, J. Power Sources 542 (2022).
[21] W. Liu, X. Hu, X. Lin, X. Yang, Z. Song, A. Foley, J. Couture, ETransportation 14 (2022).
[22] Z. Cui, L. Kang, L. Li, L. Wang, K. Wang, Renew. Energy 198 (2022) 1328–1340.
[23] K. Luo, X. Chen, H. Zheng, S. Zhi, J. Energy Chem. 74 (2022) 159–173.
[24] S. Arora, W. Shen, A. Kapoor, Comput. Chem. Eng. 101 (2017) 81–94.
[25] A. Legala, X. Li, Energy AI 10 (2022).
[26] Z. Cui, L. Wang, Q. Li, W.K. Wang, Int. J. Energy Res. 46 (2022) 5423–5440.
[27] X. Shu, G. Li, Y. Zhang, S. Shen, Z. Chen, Y. Liu, IEEE Trans. Transport. Electrific. 7 (2020) 1271–1284.
[28] S. Zhao, C. Zhang, Y. Wang, J. Energy Storage 52 (2022).
[29] J. Tian, R. Xiong, J. Lu, C. Chen, W. Shen, Energy Storage Mater. 50 (2022) 718–729.
[30] S. Kohtz, Y. Xu, Z. Zheng, P. Wang, Mech. Syst. Signal Process 172 (2022).
[31] B. Huang, J. Wang, IEEE Trans. Power Syst. (2022) 1–18.
[32] W. Li, J. Zhang, F. Ringbeck, D. Jost, J. Power Sources 506 (2021).
[33] M. Guo, G. Sikha, R.E. White, J. Electrochem. Soc. 158 (2011) A122-A132.
[34] L. Wu, K. Liu, H. Pang, J. Jin, Energies 14 (2021) 5265.
[35] L. Wu, H. Pang, Y. Geng, X. Liu , J. Liu, K. Liu, Int. J. Energy Res. 46 (2022) 11834-11848.
[36] J. Li, N. Lotfi, R.G. Landers, J. Park, J. Electrochem. Soc. 164 (2017) A874-A883.
[37] L. Wu, K. Liu, H. Pang, Electrochim. Acta 368 (2021).
[38] H. Yu, L. Yang, L. Zhang, J. Li, X. Liu, IScience 25 (2022).
[39] M. Farag, H. Sweity, M. Fleckenstein, S. Habibi, J. Power Sources 360 (2017) 618–633.
[40] F.K. Wang, Z.E. Amogne, J.H. Chou, C. Tseng, Energy 254 (2022).
[41] Y. Zhang, L. Tu, Z. Xue, S. Li, L. Tian, X. Zheng, Energy 251 (2022).
[42] B. Alizadeh, A. Ghaderi Bafti, H. Kamangir, Y. Zhang, D.B. Wright, K.J. Franz, J. Hydrol. 601 (2021).
[43] L. Du, R. Gao, P.N. Suganthan, D.Z. Wang, Inf. Sci. 591 (2022) 155–175.
[44] J. Ma, Y. Ding, J.C. Cheng, F. Jiang, V.J. Gan, Z. Xu, Sustain. Cities Soc. 60 (2020).
[45] F. He, J. Zhou, Z.K. Feng, G. Liu, Y. Yang, Appl. Energy 237 (2019) 103–116.
[46] G. Hwang, N. Sitapure, J. Moon, H. Lee, S. Hwang, Chem. Eng. J. 435 (2022).
[47] Q. Ding, Y. Wang, Z. Chen, J. Energy Storage 46 (2022).
[48] B. Yang, Y. Wang, Y. Zhan, Energies 15 (2022) 4670.
[49] P. Ren, S. Wang, X. Chen, H. Zhou, C. Fernandez, D.I. Stroe, Electrochim. Acta 435 (2022).
[50] L.D. Hansen, M. Stokholm-Bjerregaard, P. Durdevic, Comput. Chem. Eng. 160 (2022).
[51] X. Ren, S. Liu, X. Yu, X. Dong, Energy 234 (2021).
[52] Z. Cui, L. Kang, L. Li, K. Wang, Energy 259 (2022).
[53] X. Zhang, P. Li, B. Huang, H. Zhang, Int. J. Heat Mass Transf. 199 (2022).
[54] M. Xu, X. Wang, L. Zhang, P. Zhao, Energy 227 (2021).
[55] E. Prada, D. Di Domenico, Y. Creff, J. Bernard, V. Sauvant-Moynot, F. Huet, J. Electrochem. Soc. 159 (2012) A1508-A1519.
[56] C. Heubner, M. Schneider, A. Michaelis, J. Power Sources 307 (2016) 199–207.
[57] J. Kang, Y. Jia, G. Zhu, J. Wang, B. Huang, Y. Fan, J. Energy Storage 46 (2022).
[58] E. Catenaro, S. Onori, Data Brief 35 (2021).
[59] F. Feng, S. Teng, K. Liu, J. Xie, Y. Xie, B. liu, K. Li, J. Power Sources 455 (2020).
[60] Y. Tian, R. Lai, X. Li, L. Xiang, J. Tian, Appl. Energy 265 (2020).
[61] S. Yang, S. Zhou, X. Zhou, Y. Lu, X. Liu, H. Yang, Y. Pan, X. Yang, L. Xiao, X. Tang, P. Hu, J. Energy Storage 52 (2022).